IEEE Access
Multidisciplinary | Rapid Review | Open Access Journal

Received February 28, 2020, accepted March 14, 2020, date of publication March 19, 2020, date of current version March 30, 2020.

Digital Object Identifier 10.1109/ACCESS.2020.2981947

Remaining Useful Life Estimation of Lithium-Ion Batteries Based on Optimal Time Series Health Indicator

ZHONGHUA YUN AND WENHU QIN
School of Instrument Science and Engineering, Southeast University, Nanjing 210096, China

Corresponding author: Wenhu Qin (qinwenhu@seu.edu.cn)

This work was supported in part by the Key R&D Program of Jiangsu Province under Grant BE2019311, in part by the Fundamental Research Funds for the Central Universities under Grant 2242019k30043, and in part by the Key Research and Development Program of Jiangsu Province under Grant BE2017035.

ABSTRACT The evaluation of lithium battery performance is a complex and very important issue. Generally, manufacturers perform battery burn-in tests and evaluate the performance of lithium batteries based on capacity, internal resistance, voltage, and other parameters in the cycle. However, due to the complexity of practical applications and the difficulty of parameter measurement, it is necessary to evaluate the status of health (SOH) of lithium-ion batteries from the side. Analysis of battery charge and discharge data found that using the charge and discharge time to evaluate the health of the battery is effective and feasible, especially the time during the discharge/charge platform period, and the parameter measurement is more convenient. In this paper, three time-health indicators are constructed and analyzed in detail, and then the health of the battery is evaluated using a simple Bayesian Monte Carlo theory. The experimental results of four batteries show that the scheme is simple and convenient, and can effectively evaluate the SOH of lithium-ion batteries.

INDEX TERMS Optimal health indicator, lithium-ion battery, correlation analysis, time difference, Bayesian Monte Carlo, state of health.

I. INTRODUCTION

In recent years, non-renewable energy sources such as oil have gradually been exhausted, therefore, the research in electric vehicles and hybrid vehicles has been intensified around the world and it will be regarded as the important vehicle models in the future. Because lithium-ion batteries can store electrical energy in the form of chemical energy and can be reused, therefore, it can be widely used in various industrial and civil fields such as electric vehicles, mobile devices, drones according to different specifications. The main advantages of lithium-ion batteries are high energy density, low self-discharge rate, long life, etc.However, it cannot discharge at a large current and has the disadvantage of poor safety, therefore, the deterioration monitoring of lithium-ion batteries and the prediction of remaining useful life are extremely important in practical applications. Generally, the health indicator of the battery is the releasable capacity, but it is not convenient to calculate, so a better indicator is needed to characterize the State-of-Health (SOH) from the side, and this is important for lithium battery health management and reliability. In essence, the more accurate and reliable the predictions, the users can maintain the system promptly to ensure safety and avoid disasters.

Many scholars conducted research work on degradation modeling and Remaining Useful Life (RUL) prediction in past years. Saha *et al.* used particle filter to study the Remaining Useful Life prediction of the battery algorithm [1], [2]. He *et al.* [3]. studied the health status and remaining service life of lithium-ion batteries using the Dempster-Shafer theory and Bayesian Monte Carlo theory, respectively. Wang *et al.* [4], Xing *et al.* [5], and Liu *et al.* [6] used the correlation vector machine and three-parameter capacity degradation model, combines empirical exponential and a poly-nominal regression model and particle filtering, the Grey Correlation Analysis and Ensemble MONotonic Echo State Network algorithm to track the battery's degradation trend and predicted the RUL of battery, respectively.

The associate editor coordinating the review of this manuscript and approving it for publication was Eklas Hossain.

Hu *et al.* [7] used the Gauss–Hermite particle filter technique to project the capacity fade to the end-of-service value or the failure limit for the RUL prediction. Liu *et al.* [8], [9] used the discharging voltage difference of equal time interval and an optimized relevance vector-machine algorithm, combines the battery capacity and time interval of equal discharging voltage and a data-driven monotonic echo state networks algorithm to track the nonlinear patterns of battery degradation, respectively. Zhou *et al.* [10] and Huang *et al.* [11] used the mean voltage falloff and discharging cycle, instantaneous discharging voltage and the unit time voltage drop to estimations the state-of-health of Li-ion batteries, respectively. Su *et al.* [12] and Ren *et al.* [13] studied the interacting multiple model particle filter, integrating the auto encoder with deep neural network (DNN) for RUL prediction of lithium-ion battery. Sun *et al.* incorporating capacitance, resistance, and constant current charge time used particle filter algorithm to predict remaining useful life [14]. Power attenuation is difficult to study, so it is usually reflected by internal impedance or other factors [15],. Wei *et al.* used the impedance variables and Particle Filter and Support Vector Regression to estimate the impedance degradation parameters [16]. Sun *et al.* presents that the order of stress factors in terms of significance for cycle life derating is temperature > charge/discharge C-rate > charge cut-off current > charge cut-off voltage [17]. Saxena *et al.* used an accelerated fade model under multiple C-rate loading conditions and a nonlinear mixed-effects regression to consider the variability of repeated capacity measurements [18]. Lee *et al.* detecting anomalies before EOL to reducing the time for the qualification test of Li-ion batteries [19]. Zhang *et al.* [20], [21], and Cadini *et al.* [22] combines the relevance vector machine and particle filter, Box–Cox transformation and the Monte Carlo simulation, and particle filtering and neural networks to estimate the remaining useful life, respectively. Zhu *et al.* [23] investigated through experiments that the Effect of the alternating current pulse heating method on battery SoH for large laminated power lithium-ion batteries, and indicates that the AC heating method does not aggravate the battery degradation.

Generally, the internal mechanism of the battery involves many complicated factors such as materials and chemical reactions, but it is not convenient to monitor these internal parameters in the application environment. Therefore, it requires a simple and unambiguous estimation of the remaining useful life and the state of health of lithium-ion batteries from the side. Besides, the measurement of the battery capacity requires the use of complex integration operations, this increases computational costs. And it is difficult to accurately monitor the temperature due to the temperature change of the battery itself as well as the ambient temperature and sensor position. Therefore, it is necessary to study a simpler evaluation scheme for the SOH of the batteries.

In this paper, the research on the degraded dataset of lithium-ion batteries is carried out from the perspective of time, extract the time variable as a health indicator and compared with the voltage. Then the relationship between time variables and capacity degradation was studied by correlation analysis, and the optimal health indicator was used after analysis. Besides, to compare with the capacity indicator, experiments were performed on four batteries using a simple Bayesian Monte Carlo method as a prediction algorithm.

Experimental results show that using optimal time difference indicator (discharge/ charge/hybrid) to estimate the state of health of the lithium-ion battery and the life prediction track of lithium-ion battery more accurately. Besides, since the difference between two values is used, it is not necessary to align the sampling frequency, which is also one of the advantages of using time difference as a health indicator in this paper. This scheme is suitable for occasions lacking precision equipment.

The rest part of the paper is organized as follows: Section II analyzes the dataset, extracts the capacity series, time series, voltage series data. Section III establishes a health indicator based on time series and conducted correlation analysis to select the optimal health indicator. Section IV details the Bayesian Monte Carlo theory based on time series health indicators. Section V gives the experimental results of the SOH predicts based on time series health indicator and capacity series health indicator for comparison. Section VI gives the discussion of the experiment. Finally, the Conclusions are drawn in Section VII.

II. ANALYSIS OF THE EXPERIMENTAL DATASET

The dataset was selected from the dataset Battery Aging ARC-FY08Q4 provided by the Prognostics CoE at National Aeronautics and Space Administration (NASA) Ames Research Center [24]. It includes 3 different operational profiles for charging, discharging and impedance of 4 lithium-ion batteries (#05, #06, #07 and #18) operating at room temperature. The charging was carried out in a constant current of 1.5 A until the battery voltage reached 4.2 V, and a constant voltage was maintained to charging until the current reduced to 20 mA. The discharge at a constant current of 2A until the voltage drops to 2.7V, 2.5V, 2.2V, and 2.5V, respectively. When the capacity of the battery has been degraded by 30% (from 2 Ahr to 1.4 Ahr), the experiment is stopped.

Select the experimental data of 4 batteries(#05, #06, #07, and #18) in the battery data set and plot the capacity data as shown in Fig.1. As can be seen from Fig.1, the new lithium-ion battery has the largest discharge time after being fully charged. However, as the battery is repeatedly charged and discharged, a variety of complex causes decay in the amount of electricity that can be released such as the passivation film increases, the active material particles fall off, the lattice collapse of the active material, etc, this phenomenon is also called battery degradation. Taking the #06 battery as an example, the relationship

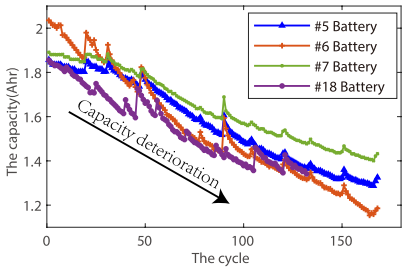

FIGURE 1. Capacity degradation curves of 4 batteries (ARC-FY08Q4-B006).

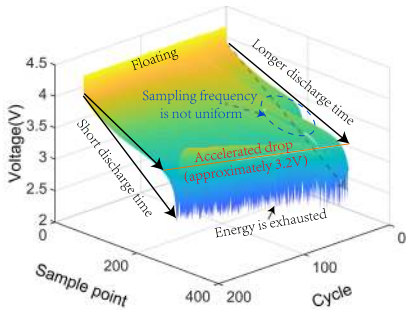

FIGURE 2. Relationship between battery voltage and sampling point time during different cycles (Discharge curve).

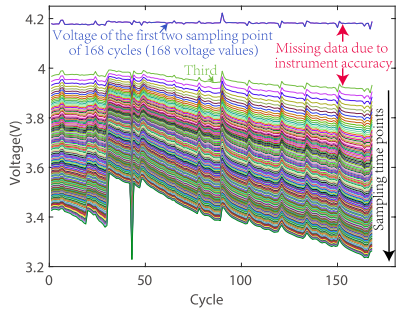

(a)

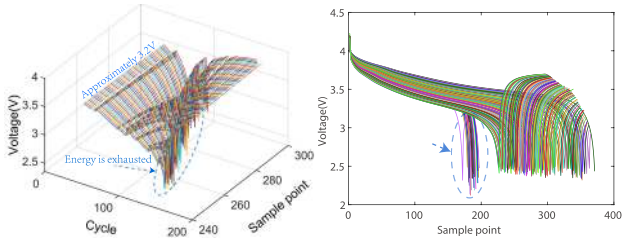

(b) (c)

FIGURE 3. Voltage changes in each cycle: (a) first 200 sampling points (about 200 curves, each represents voltage at same sampling point in 168 cycles), (b) energy is about to be exhausted, (c) relationship between voltage and sampling time point in 168 cycles (168 curves).

between its working voltage, sampling time and the number of cycles are shown in Fig.2.

About 200 curves of the voltage change of the first 200 or so sampling points (corresponds to the first 200 columns in the right half of Table 1) are shown in Fig.3a, the voltage near the moment when the energy of the energy is about to be exhausted in each cycle are shown in Fig.3b. It can be

TABLE 1. The time and the voltage of the same sample point(#06 battery).

cycle	The sample point /sec				The sample voltage / V			
	1	2	3	4	1	2	3	4
28	0	16.641	35.594	53.734	4.17626	4.17592	3.96863	3.94771
29	0	16.734	35.625	53.859	4.18818	4.18816	3.98010	3.95864
31	0	9.39	19.578	28.937	4.18980	4.18999	3.99257	3.97755
32	0	9.375	19.562	28.984	4.18694	4.18698	3.99259	3.97763

Raw data are from Prognostics CoE at NASA Ames Research Center.

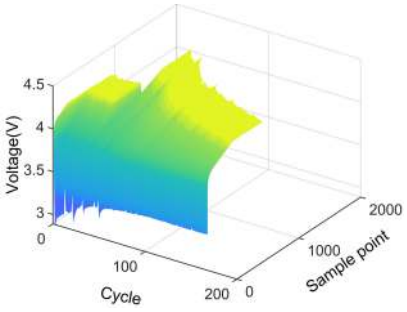

FIGURE 4. Relationship between battery voltage and sampling point time during different cycles(charging process).

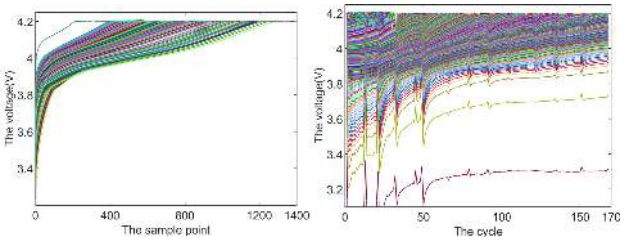

(a) (b)

FIGURE 5. The charging process curve contains 3900 sampling points. (a): the first 1300 sampling points. (b): curves 1, 2, 3, 6, 9, ...3897, 3900.

seen from Fig.3a that as the battery is repeatedly charged and discharged, the voltage at the same sampling instant of each cycle tends to decrease faster and faster, for example, the top curves of Fig.3a exhibits a near-horizontal characteristic, while a lowermost curve exhibits a steeper feature. The curves of the battery voltage in each cycle are shown in Fig.3c, the 168 curves in Fig.2 and Fig.3c represent the changes in voltage during 168 cycles, respectively, the sampling points during each cycle are inconsistent from 180 to 371. In addition, the voltage drops in cycle1 to cycle 30 and cycle 43 faster than other cycles in Figures 2 and 3c. After analyzing the battery data provided by NASA, it was found that this was caused by different sampling frequencies, except for these cycles, the other sampling time points were almost the same, since the difference between the two values is used, it is not necessary to align the sampling frequency in Fig.2 (as shown by the cycle 1 to 30 and 43 in Fig. 2 and 3c).

Similar to the discharge process, the main charging process (about 3.5V to 4.2V) is shown in Fig.4 and the characteristic curves during the charging process are shown in Fig.5. As can be seen from Fig.2 and Fig.4, as the cycle increases, the rate

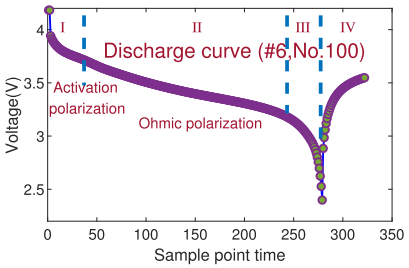

FIGURE 6. Discharge curve of the 100th cycle (#06 battery).

of battery voltage drop/rise will accelerate, that is, the time required to discharge/charge will be shortened.

III. HEALTH INDICATOR EXTRACTION AND THE CORRELATION ANALYSIS

A. HEALTH INDICATOR EXTRACTION AND SELECTION

Combined with the analysis in section II, as can be seen from Fig.3a and Fig.5a, as the deterioration of the battery becomes serious, the battery discharge time and the fully charge time will be shorter. Therefore, it can consider using the battery's charge/discharge time as a battery health indicator. This needs to select as the start point and the endpoint, but the data of the battery monitored by the instrument is often unsatisfactory at the beginning of discharge, this is mainly caused by the battery itself and the equipment factor, etc. In Fig.3a, there are large blanks present at the first few sampling points, and from the analysis of the raw data of NASA, the first point is near the starting voltage of about 4.2V, and the voltage from the third sampling point is lower than 4V, it is between 3.99V and 3.98V and 3.89V.

Taking the #06 battery as an example, the time and voltage are extracted for research, as shown in Table 1 (only a small part of the data is listed), the voltages and sampling times of the first to fourth sampling points in cycle 28 to cycle 32 are listed in this table. As can be seen from Fig.3a and Table 1, there are only two data of the voltage dropped from 4.2V to 4V, besides, the data is complicated and inconvenient to use when the battery is exhausted as shown in Fig.3b.

B. QUALITATIVE ANALYSIS OF DISCHARGE TIME DIFFERENCE HEALTH INDICATOR

From basic characteristics of battery, the battery discharge process is mainly divided into 3 stages. The first stage is the period of rapid voltage drop, about from the initial voltage drop to 4V. The second stage is the platform period of discharge, it is steadily decreasing from about 4V to 3.2V. The third stage is the voltage drops sharply until the cut-off voltage of the battery. The schematic diagram of discharge process shows in Fig.6.

From the above analysis and Fig.6, it can be seen that both the second and third phases are more likely to collect more data, in the second stage, the magnitude of the voltage change is small, but the time varies greatly, considering that in applications, lithium batteries usually work during the second stage, so it is more suitable to monitor the SOH of lithium

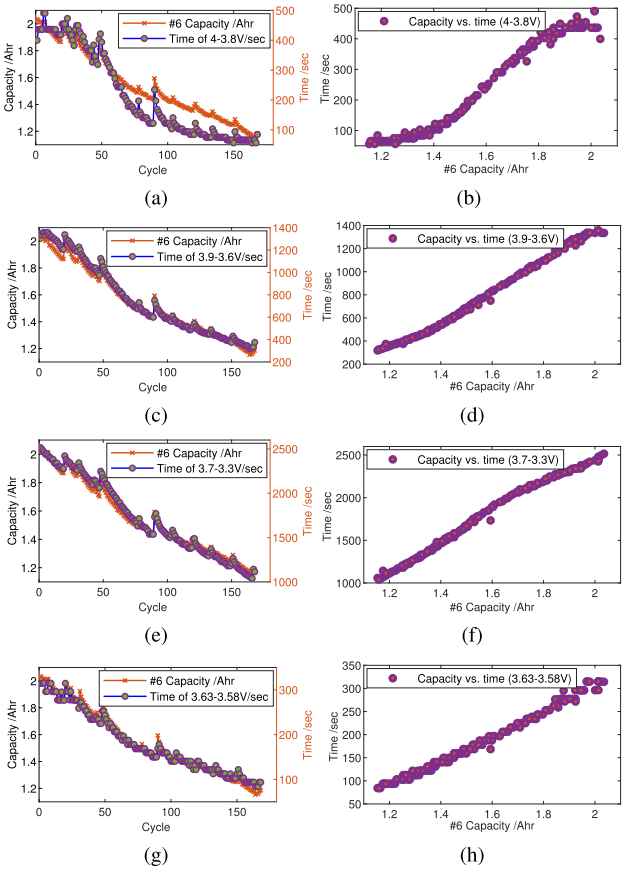

FIGURE 7. Experimental curves: (a,c,e,g) Time required for different voltage drops and the capacity. (b,d,f,h) The relationship between them.

batteries during the platform period of discharge from the perspective of time. To research the broad applicability of time health indicator, four batteries (#05, #06, #07 and #18) were used for experiments to investigate the arbitrariness of the voltage drop range. Taking 4V-3.8V, 3.9V-3.6V, 3.7V-3.3V, and 3.63V-3.58V as examples, which correspond to voltage drops of 0.2V, 0.3V, 0.4V, and 0.05V, respectively, the correlation analysis are shown in Fig.7.

From the analysis, it can be found that the four curves all have a high correlation with the capacity degradation curve, therefore, the change of the time required for the voltage drop can reflect the deterioration in the battery, that is, the global degradation characteristics of the battery. The time required for the voltage to decrease slightly and the capacity degradation curve of battery #05, #07 and #18 are no longer given (similar to Figures.7a, 7c, 7e, and 7g).

C. CORRELATION ANALYSIS OF HEALTH INDICATOR

In statistics, Kendall's tau correlation coefficient (Kendall's tau), Pearson's linear correlation coefficient (Pearson's r), Spearman's rank correlation coefficient (Spearman's rho) can be used for statistical analysis of Norminal Data, Interval Data and Ordinal Data, which can be used to analyze the Linear trends and monotonous trends of the data [25], [26].

Kendall tau rank correlation coefficient (Kendall's tau) is used to measure the association between the time required and capacity degradation quantities to establish whether two variables may be regarded as dependent, the advantage of this test is it doesn't rely on any assumptions on the distributions of X or Y. If the agreement between the two rankings, the coefficient has value 1, if the disagreement between the two rankings, the coefficient has value -1, if X and Y are independent, the coefficient approximately equal to zero. This coefficient τ can be written as Equations 1.

$$\left.\begin{aligned} \tau &= \frac{K}{\frac{1}{2}n\left(n-1\right)}, \\ K &= \sum_{i=1}^{n-1}\sum_{j=i+1}^{n}\xi^*\left(Xa,i,Xa,jYb,i,Yb,j\right) \\ &\xi^*\left(Xa,i,Xa,jYb,i,Yb,j\right) \\ &= \begin{cases} +1, & \left(Xa,i-Xa,j\right)\left(Xa,i-Xa,j\right)>0 \\ 0, & \left(Xa,i-Xa,j\right)\left(Xa,i-Xa,j\right)>0 \\ -1, & \left(Xa,i-Xa,j\right)\left(Xa,i-Xa,j\right)>0 \end{cases} \end{aligned}\right\} \quad (1)$$

The Spearman correlation coefficient (Spearman's rho) is defined as the Pearson correlation coefficient between the ranked variables can be written as Equation 2, it is a non-parametric measure of statistical dependence between two variables, it can be used to evaluate whether the relationship between the time required for discharge and the lithium battery capacity reduction data is monotonic.

$$\rho_{rg_X,rg_Y} = \frac{cov\left(rg_X,rg_Y\right)}{\sigma_{rg_X}\sigma_{rg_Y}} \quad (2)$$

In this equation, ρ denotes the usual Pearson correlation efficient, $cov\left(rg_X,rg_Y\right)$ is the covariance of the rank variables are the standard deviations of the rank variables, $\sigma_{rg_X},\sigma_{rg_Y}$ are the standard deviations of the rank variables, if all n ranks are distinct integers (n is the number of observations), it can be calculated by Equations 3.

$$\left.\begin{aligned} \rho\left(a,b\right) &= 1-\frac{6\sum d_i^2}{n(n^2-1)} \\ d_i &= rg\left(X_i\right)-rg\left(Y_i\right) \end{aligned}\right\} \quad (3)$$

The pearson correlation coefficient (Pearson's r) $\rho_{X,Y}$ of the variables (X, Y) is equal to the covariance cov(X, Y) divided by the product of their respective standard deviations $(\rho_X \cdot \rho_Y)$, it can be written as Equation 4.

$$\left.\begin{aligned} \rho_{X,Y} &= \frac{cov\left(X,Y\right)}{\sigma_X\sigma_Y} \\ &= \frac{E\left(XY\right)-E\left(X\right)E\left(Y\right)}{\sqrt{E\left(X^2\right)-E^2\left(X\right)}\sqrt{E\left(Y^2\right)-E^2\left(Y\right)}} \\ &= \frac{\sum XY-\frac{\sum X\sum Y}{N}}{\sqrt{\left(\sum X^2-\frac{\left(\sum X\right)^2}{N}\right)\left(\sum Y^2-\frac{\left(\sum Y\right)^2}{N}\right)}} \end{aligned}\right\} \quad (4)$$

The correlation coefficient has a value between -1.0 and 1.0, the larger the absolute value, the stronger the negative/positive correlation, and the closer the correlation is to zero, the weaker the correlation, or the correlation can be quantified to several degrees, where $\rho > 0$ represents the positive correlation between the two variables and $\rho < 0$ represents the negative correlation between two variables; when $|\rho| >= 0.8$, the two variables can be considered highly correlated; when $0.8 > |\rho| >= 0.5$, the two variables can be considered moderately correlated; and $0.5 > |\rho| >= 0.3$ regarded as low-level correlation; when $|\rho| < 0.3$, the correlation is considered weak or even irrelevant (assuming the correlation is expressed by r). Here, it is taken as a measure of the correlation between time series and capacity degradation.

TABLE 2. Correlation between time difference and capacity degradation.

voltage /V	CC (#05)			CC (#06)		
	K	P	S	K	P	S
Max to 4.0	0.5712	0.8926	0.7878	0.3408	0.7266	0.4903
max to 4.1	0.3263	0.6236	0.4768	0.3408	0.7266	0.4903
4.1 to 4.0	0.2986	0.4488	0.3947	NaN*	NaN	NaN
4.0 to 3.9	0.8048	0.9642	0.9370	0.8413	0.9646	0.9636
3.9 to 3.8	0.8646	0.9860	0.9645	0.9136	0.9800	0.9876
3.8 to 3.7	0.9156	0.9728	0.9898	0.9586	0.9931	0.9972
3.7 to 3.6	0.9414	0.9954	0.9936	0.9574	0.9921	0.9968
3.6 to 3.5	0.9429	0.9973	0.9909	0.9695	0.9873	0.9982
3.5 to 3.4	0.8816	0.9741	0.9650	0.9430	0.9829	0.9921
3.4 to 3.3	-0.8879	-0.9915	-0.9778	-0.2752	-0.7322	-0.4867
3.3 to 3.2	-0.8655	-0.9667	-0.9633	-0.8677	-0.9712	-0.9698
3.2 to 3.1	-0.7821	-0.9519	-0.9330	-0.8757	-0.9679	-0.9754
3.1 to 3.0	-0.7214	-0.9249	-0.8971	-0.7768	-0.9585	-0.9441
3.0 to 2.9	-0.6872	-0.9188	-0.8736	-0.7051	-0.9424	-0.8951
2.9 to 2.8	-0.4502	-0.7802	-0.6956	-0.4435	-0.7468	-0.6925
2.8 to 2.7	-0.0949	-0.3599	-0.1079	-0.1504	-0.5135	-0.1889
2.7 to 2.6	-	-	-	-0.0113	-0.2676	-0.0414
2.6 to 2.5	-	-	-	-0.0949	-0.3240	-0.1478

Here, "CC" means "Correlation coefficient", "K" means "Kendall's tau ", "P" means "Pearson's r ","S" means "Spearman's rho "

TABLE 3. Correlation between time difference and capacity degradation.

voltage /V	CC (#07)			CC (#18)		
	K	P	S	K	P	S
3.9 to 3.8	0.8608	0.9719	0.9652	0.8650	0.9712	0.9721
3.8 to 3.7	0.9045	0.9733	0.9863	0.8760	0.9750	0.9785
3.7 to 3.6	0.9343	0.9961	0.9921	0.9313	0.9967	0.9934
3.6 to 3.5	0.9165	0.9920	0.9798	0.9468	0.9967	0.9955
3.5 to 3.4	0.8973	0.9533	0.9794	0.9146	0.9812	0.9863
3.4 to 3.3	-0.8629	-0.9669	-0.9620	-0.8499	-0.9751	-0.9598

Using the voltage drop of 0.1V as a Benchmark, the correlation coefficients (CC) of the time difference sequence and capacity degradation sequence are shown in Table 2 and 3.

It can be seen that the two highest correlation coefficients of the #05 and #06 batteries correspond to the time required for the voltage drop from 3.6V to 3.5V, and the highest correlation coefficient of #07 battery and #18 battery corresponds to the time required for the voltage to drop from 3.7V to 3.6V and from 3.6V to 3.5V, respectively. Similar to Table 2, the key correlation coefficients are listed in Table 3.

However, the time series health indicator corresponding to different ranges of voltage drop are also different. In order to study this problem, 3 correlation coefficients of four voltages of 3.63-3.58V, 3.7-3.3V, 3.9-3.6V and 4-3.8V are selected, and a total of 48 data for research, these correlation coefficients are shown in Table 4. It can be found that only

TABLE 4. Correlation between time difference and capacity degradation.

CC		Time required for different voltage drops			
		4 to 3.8	3.9 to 3.6*	3.7 to 3.3	3.63 to 3.58
Kendall's tau	#05	0.8626	0.9567	0.9739	0.9035
Pearson's r		0.9843	0.9977	0.9984	0.9921
Spearman's rho		0.9591	0.9941	0.9984	0.9857
Kendall's tau	#06	0.9198	0.9790	0.9825	0.9453
Pearson's r		0.9790	0.9965	0.9959	0.9954
Spearman's rho		0.9880	0.9990	0.9993	0.9957
Kendall's tau	#07	0.8837	0.9636	0.9682	0.9031
Pearson's r		0.9814	0.9985	0.9981	0.9928
Spearman's rho		0.9720	0.9968	0.9977	0.9851
Kendall's tau	#18	0.8730	0.9549	0.9579	0.8714
Pearson's r		0.9693	0.9974	0.9957	0.9900
Spearman's rho		0.9708	0.9961	0.9967	0.9779

Here, experimental scheme was slightly modified of the voltage drops from 3.9V to 3.6V of the battery #07 and #18 (see section V for details).

the Kendall's tau of the 0.2V volt drop are higher than the correlation coefficient of 0.05V volt drop of the #18 battery, but all other correlation coefficients of less than 0.05V volt drop, this is due to the uncertainty of the initial actual voltage caused by the uncertainty initial floating state of the battery.

From the analysis above, it can be concluded that the correlation is related to the voltage range. According to the characteristics of lithium batteries, the discharge voltage is a process of decreasing, stable, and rapid decreasing (similar to Fig.6), wherein a battery with a long stable period and a high discharge platform is better, which is related to the manufacturing process. Therefore, using the dischargeable time duration within the discharge platform period as the health indicator can better reflect the deterioration condition of the lithium battery, similar conclusions were reached after analyzing different time horizons. Besides, using strongly correlated data can better represent the degradation status of lithium batteries. It can be found in Table 4 that although the 3.7-3.3V interval includes the 3.4 to 3.3V interval that is not highly correlated, the three correlation coefficients are 0.9825, 0.9959, and 0.9993. Therefore, the interval of 3.7-3.3V can still well characterize the SOH of lithium batteries.

Therefore, in practical applications, the voltage range should be as close as possible to the center of the platform area or use several voltage ranges separately to comprehensively evaluate the health status of the lithium battery. In this paper, we will experiment with these four voltage ranges as examples, and the subsequent experimental results also verify the robustness and applicability of the method.

D. ANALYSIS OF CHARGE TIME DIFFERENCE HEALTH INDICATOR AND HYBRID HEALTH INDICATORS

Similar to sectionIII-B, as can be seen from Figures 3 and 5 that the charging process also includes several stages. First, the voltage will rise quickly to around 3.8V; next, it will stabilize to 4.2V after a long time of charging; finally, the voltage is maintained at 4.2V to continue charging. Therefore, similar to Tables 2 and 3, the correlation analysis of the voltage range from 3.6V to 4.2V is shown in Tables 5 and 6. From Table 5 and 6, it can be seen that the correlation

TABLE 5. Correlation between time difference and capacity degradation.

voltage /V	CC (#05)			CC (#06)		
	K	P	S	K	P	S
3.7 to 3.8	0.7646	0.8645	0.8877	0.4577	0.8298	0.5943
3.8 to 3.9	0.8694	0.9569	0.9421	0.8916	0.9338	0.9482
3.9 to 4.0	0.8887	0.9428	0.9468	0.9127	0.9497	0.9539
4.0 to 4.1	0.8639	0.7781	0.9329	0.8701	0.8851	0.9363
4.1 to 4.2	0.8173	0.9168	0.9198	0.6382	0.7757	0.7889

TABLE 6. Correlation between time difference and capacity degradation.

voltage /V	CC (#07)			CC (#18)		
	K	P	S	K	P	S
3.6 to 3.7	0.5820	0.8361	0.7509	0.4417	0.6085	0.5754
3.7 to 3.8	0.8398	0.9290	0.9312	0.5549	0.5863	0.6976
3.8 to 3.9	0.8530	0.9376	0.9338	0.6611	0.7086	0.7818
3.9 to 4.0	0.8691	0.8952	0.9383	0.8295	0.8463	0.9111
4.0 to 4.1	0.8293	0.5366	0.9198	0.7969	0.6870	0.8962
4.1 to 4.2	0.7103	0.8088	0.8429	0.7490	0.8355	0.8779

TABLE 7. Correlation between time difference and capacity degradation.

CC		Time required for different voltage drops				
		4.0 to 3.7	4.1 to 3.9	4.0 to 3.8	3.9 to 3.7	3.93 to 3.88
K	#05	0.8870	0.9029	0.8868	0.8718	0.8694
P		0.9533	0.9099	0.9515	0.9497	0.9522
S		0.9472	0.9507	0.9469	0.9432	0.9419
K	#06	0.9080	0.9172	0.9090	0.8878	0.8968
P		0.9454	0.9419	0.9481	0.9203	0.9462
S		0.9526	0.9566	0.9528	0.9473	0.9493
K	#07	0.8690	0.8958	0.8701	0.8571	0.8557
P		0.9227	0.8314	0.9140	0.9446	0.9116
S		0.9388	0.9466	0.9384	0.9355	0.9344
K	#18	0.7645	0.8765	0.7783	0.6371	0.7467
P		0.8093	0.8187	0.8195	0.6878	0.7787
S		0.8750	0.9328	0.8836	0.7493	0.8679

coefficient is the greatest when the voltage is around 3.8V, 3.9V, 4.0V.

Similar to the discharge process, calculate the correlation coefficients as shown in table 7, these 5 intervals roughly cover the voltage difference of 0.3V, 0.2V and 0.05V near the maximum correlation interval in Table 5 and 6.

Fig. 8 shows the relationship between the capacity and the time required for the three types of voltage rise (3.7V-4.0V, 3.9V-4.1V, 3.88-3.93V). It can be clearly seen that there is an outlier in this Figure, which is because the new battery already has power when it is first charged. Therefore, the time of the first charge is independent of the trend of these curves.

Next, consider hybrid health indicators. From the above analysis, it can be known that both the charging time difference and the discharging time difference can characterize the health status of the battery. To fully reflect the charge/discharge characteristics, combine the charge time difference and discharge time difference health indicators into a new health indicator. In the selection interval, according to the previous correlation analysis results, consider types of indicators, a hybrid indicator covers the charging time from 3.9V to 4.1V and the discharging time from 3.7V to 3.4V, another is 3.7V-3.9V / 3.9V-3.7V. The results are shown

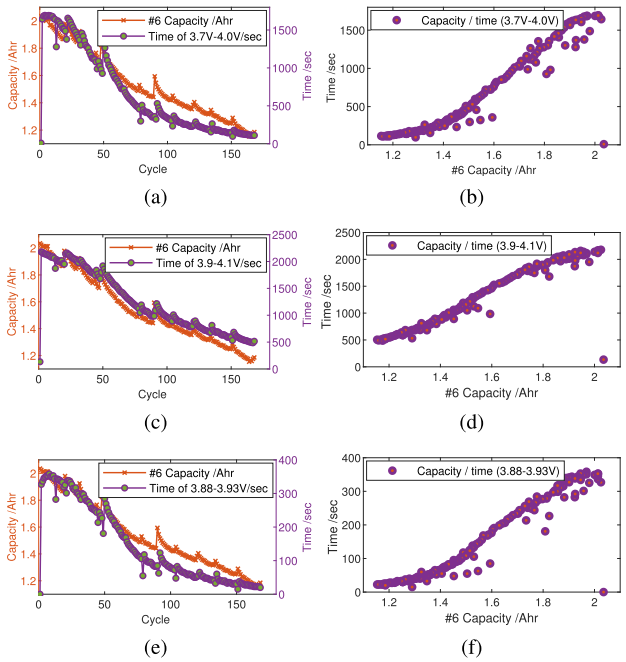

FIGURE 8. Experimental curves: (a) 3.7V-4.0V and capacity. (c) 3.9V-4.1V and capacity. (e) 3.88V-3.93V and capacity. (b,d,f) relationship.

TABLE 8. Correlation coefficient between hybrid health indicators and capacity degradation.

	K	P	S	K	P	S
	(3.9-4.1V/3.7-3.4V)			(3.7-3.9V/3.9-3.7V)		
Bat #05	0.9367	0.9723	0.9663	0.9146	0.9801	0.9789
Bat #18	0.9146	0.9495	0.9483	0.7696	0.8989	0.8903

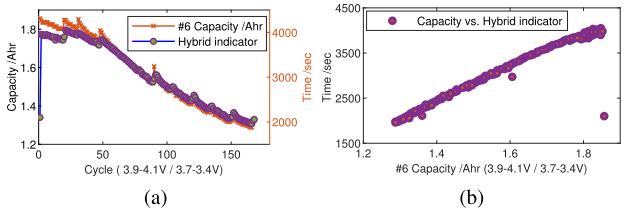

FIGURE 9. Experimental curves: (a) Time required for voltage drops from 3.9V to 4.1V / 3.7V-3.4V and the capacity. (b) Relationship between them.

in Table 8 and Fig.9. Only the experimental results of the battery #05 and #06 are given here, the others are similar.

Because the hybrid health indicator takes into account both the discharge process and the charging process, it can comprehensively characterize the battery degradation state.

E. THE VOLTAGE DIFFERENCE HEALTH INDICATOR

Next take the discharge process as an example to analyze the impact of monitoring accuracy. Since it is impossible to know in advance what voltage value the battery will reach at some point during the discharge process, therefore, the voltage drop during the period from 500 seconds to 1000 is selected as an example for the analysis of the health indicator. To simulate the actual situation, take the accuracy of voltage 0.1V, time accuracy of 1 second, part of the raw data is processed as

TABLE 9. Part of the processed data and comparison table 1(Discharge).

cycle	Time /sec				Sample voltage / V			
	1	2	3	4	1	2	3	4
29	0	16	35	53	4.1000	4.1000	3.9000	3.9000
32	0	9	19	28	4.1000	4.1000	3.9000	3.9000
33	0	9	19	29	4.1000	4.1000	3.9000	3.9000

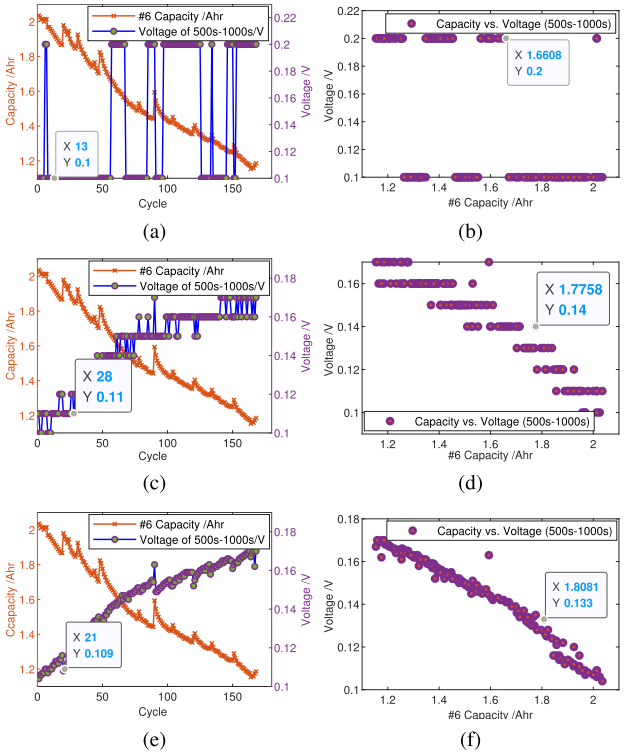

FIGURE 10. Experimental curves of voltage drop health indicator of #06 battery: (a-b) 1s and 0.1V, (c-d) 1s and 0.01V, (e-f) 1s and 0.001V.

shown in Table 9 (corresponds to Fig.10(a) and Fig.10b) to compare Table 1.

Although the voltage value at a certain time during battery discharge cannot be obtained in advance, however, it can be known from the test data that the voltage around 500s is about 3.7V, and the voltage drops to about 3.6V at 1000s when the accuracy of 0.1V and one second is selected. Therefore, a time interval of 500s to 1000s (corresponding to 3.7V to 3.6V) can be selected to analyze the performance of two health indicators. To further research, two types of voltages accuracy 0.01V and 0.001V are also selected and the time precision is in units of one second. The results are shown in Fig.10. In addition, experiments were performed with a time accuracy of 0.1 s and 0.01 s and a voltage accuracy of 0.01V. The results are shown in Fig.11.

Through the above experiments, it can be seen that the accuracy of the voltage seriously affects the correlation results of the health indicator, but the accuracy of the time has little effect on the correlation. The reason for this phenomenon is that the voltage of the battery is only reduced from 3.2V to 2.5V during the entire discharge cycle, only a voltage drop of 1.5V. But the actual discharge time of a

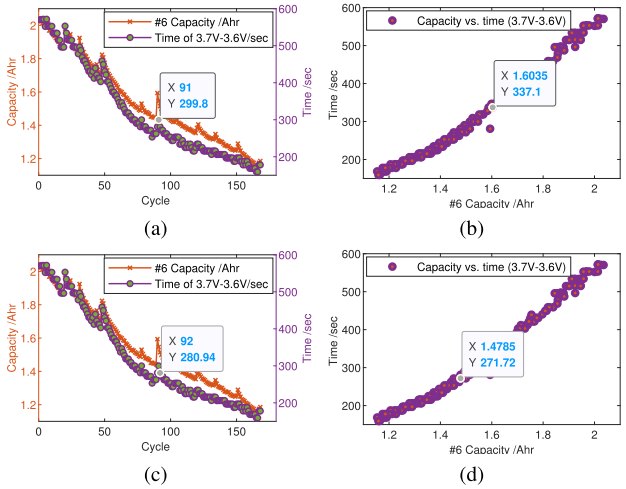

FIGURE 11. Experimental curves of time difference health indicator of #06 battery: (a-b) 0.1s and 0.01V (c-d) 0.01s and 0.01V.

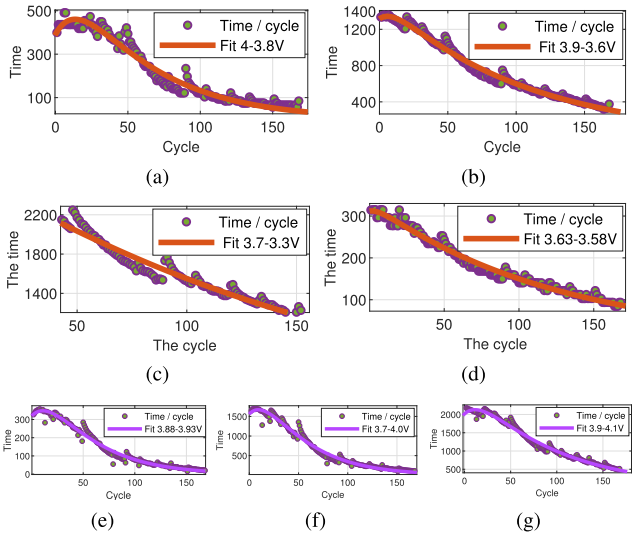

FIGURE 12. Fit curves of the time series (#06): (a-d) discharge process, (e-g) charge process.

battery is usually hundreds of seconds, thousands of seconds, even tens of thousands of seconds, if the battery runs out of power in a short time, it may be due to the battery's severe aging, or the battery capacity selection is inappropriate.

Although high-voltage accuracy and high-time accuracy acquisition are helpful for lithium battery monitoring, this requires high-precision equipment. Besides, high-frequency sampling will cause a large amount of unnecessary data, which will cause the problem of the insufficient computing capacity of the system. Based on the above analysis results, the time difference health indicator has a clear advantage over the voltage drop health indicator in the actual battery management system.

IV. THE BAYESIAN MONTE CARLO THEORY BASED ON TIME SERIES HEALTH INDICATOR

A. THE MODEL OF TIME SERIES HEALTH INDICATOR

After multiple fittings to time sequence Health Indicator, the fitting effect of double exponential model and the time difference series data is more consistent. Still taking the battery #06 as an example, the seven fitting curves of the time required for charging/discharging are shown in Fig.12.

Perform multiple fitting experiments on the four voltage differences of the 4 batteries, the fitting curves are all similar to Fig.12, it can be seen that the fitting effect of the time series using the double exponential model $y = a_1 \times exp(a_2 \times k) + a_3 \times exp(a_4 \times k)$ is better, this is consistent with the capacity decay degradation model used by many studies. To evaluate the goodness of fit of the time series double exponential model, the R-squared adjusted (R^2_{adj}) indicator is used to evaluate the fitting effect, the R-squared adjusted is defined as Equation 5, SSE is the sum of squared error,SST is the sum of squared total, n is the number of observations, and p is the number of regression coefficients, and the RMSE of the curve is also calculated, the values are shown in Table 10.

$$R^2_{adj} = 1 - (\frac{n-1}{n-p})\frac{SSE}{SST} \tag{5}$$

TABLE 10. R^2_{adj} and RMSE of the time series double exponential model.

V/V	4-3.8	3.9-3.6	3.7-3.3	3.63-3.58	3.88-3.93	3.7-4.0	3.9-4.1
R^2_{adj}	0.9645	0.9861	0.9819	0.9803	0.9811	0.9798	0.9823
RMSE	27.45	38.77	58.78	9.64	15.7	77.15	73.89

Therefore, the state equation and the observation equation of the lithium battery time difference sequence can be modeled according to this equation. The required time difference sequence of the lithium battery can be expressed in a dynamic system, the random signal to be estimated is included in the equation of state, and the available measurement value of observation equation, usually the state-space model can be written as Equations 6.

$$\begin{cases} x_t = f(x_{t-1}, u_t) \\ y_t = g(x_t, v_t) \end{cases} \tag{6}$$

In Equations 6, x_t is the value to be estimated, f is the state transition function, u_t is the state noise, y_t is the observed value, g is the measurement function, v_t is the observation noise, so, the time difference sequence model of the lithium battery can be written as Equations 7,

$$\begin{cases} T_k = a_1 \times \exp(a_2 \times k) + a_3 \times \exp(a_4 \times k) + v_k \\ a_{i,k} = a_{i,k-1} + u_{a_i} \\ v_k \sim N(0, \sigma_T), u_{a_i} \sim N(0, \sigma_{a_i}) \end{cases} \tag{7}$$

T_k is the time required in cycle k, u and v are the Gaussian noise, a_i is the initial value which can be obtain from the experiment dataset, and we experimentally research the SOH of lithium battery based on time series by this set of equations.

B. THE BAYESIAN MONTE CARLO THEORY

In Equations 7 of Section IV-A, it needs to calculate the estimated value of ai in the kth cycle based on the

data before the k cycle, then the time required in the kth cycle can be known. Usually, the state transfer obeys the first-order Markov model, and each observation(the time difference sequence) is independent of each other. Therefore, the Bayesian formula can be used to solve the posterior probability density to obtain the optimal estimate of the future, the model can be used to predict the prior probability density and the new measurement results can be used to correct the prior probability density [27]–[31]. Since the data of the first k-1 cycles is known, the probability density of the k-1 cycle is $p(a_{k-1}|T_{k-1})$, since the parameter a and the time T are independent, the Chapman-Komolgorov Equation 9 can be obtained from the integral of the Equation 8. Here, a_k represents the state of the parameter a in Equation 7 at the Kth cycle (calculating a_1, a_2, a_3, a_4, respectively), and T_k represents the discharge time of the battery corresponding to the voltage range selected in the Kth cycle.

$$\begin{aligned} &p(a_k, a_{k-1}|T_{0:k-1}) \\ &\quad = p(a_k|a_{k-1}, T_{0:k-1})p(a_{k-1}|T_{0:k-1}) \qquad (8) \\ &p(a_k|T_{0:k-1}) \\ &\quad = \int p(a_k|a_{k-1}, T_{0:k-1})p(a_{k-1}|T_{0:k-1})da_{k-1} \\ &\quad = \int p(a_k|a_{k-1})p(a_{k-1}|T_{k-1})da_{k-1} \qquad (9) \end{aligned}$$

After obtaining the measurement time value T_k at time K, and the time value T_k at the k cycles is determined only by the parameter a_k at the k cycles, then the Bayesian formula can be used to update the prior probability to obtain the posterior probability, as shown in Equation 10.

$$\begin{aligned} p(a_k|T_{0:k}) &= \frac{p(T_k|a_k, T_{0:k-1})p(a_k|T_{0:k-1})}{p(T_k|T_{0:k-1})} \\ &= \frac{p(T_k|a_k)p(a_k|T_{0:k-1})}{\int p(T_k|a_k)p(a_k|T_{0:k-1})da_k} \end{aligned} \qquad (10)$$

It is known from the measurement equation in Equation 7 that T_k is only related to ak. Therefore, the $p(T_k|a_k)$ in Equation 10 is also called the likelihood function, and it is determined by the measurement equation and is only related to the probability distribution of the measurement noise. Since the Bayesian formula requires complex integral calculation. However, the Monte Carlo simulation method uses a large number of samples to approximate the posterior probability distribution of the variables, therefore, the summation calculation can be used to approximate the integration. Suppose that N independent and identically distributed samples $a^i_{0:k}$ can be obtained from the posterior probability density $p(a_k|T_k)$, when the value N is large enough, the frequency can approximate to the probability, then the Equation 11 can be obtained, and the δ is the Dirichlet function.

$$\hat{p}(a_{0:k}|T_{0:k}) \to \frac{1}{N}\sum_{i=1}^{N}\delta(a_{0:k} - a^i_{0:k}) \qquad (11)$$

However, even if the posterior probability density $p(a_{0:k}|T_{0:k})$ of the state is known, it is still difficult to sample. Therefore, it is necessary to introduce a probability density function that is easy to sample, that is, the importance sampling function $\pi(a_{0:k}|T_{0:k})$, and its estimate can be expressed as Equation 12. In fact, this is also the central idea of Bayesian importance sampling, that is, sampling from a reference distribution pi that is known and easily sampled. Then use the sample set obtained by sampling the reference distribution to perform weighted summation to approximate the posterior distribution $p(a_{0:k}|T_{0:k})$, and then the Equation 13 can be obtained.

$$\hat{\pi}(a_{0:k}|T_{0:k}) = \frac{1}{N}\sum_{i=1}^{N}\delta(a_{0:k} - a^i_{0:k}) \qquad (12)$$

$$\begin{aligned} &p(a_{0:k}|T_{0:k}) \\ &\quad = \int p(\xi_{0:k}|z_{0:k})\delta(\xi_{0:k} - a^i{}_{0:k})d\xi_{0:k} \\ &\quad = \int \left\{\frac{p(\xi_{0:k}|T_{0:k})}{\pi(\xi_{0:k}|T_{0:k})}\delta(\xi_{0:k} - a^i_{0:k})\right\}\pi(\xi_{0:k}|T_{0:k})d\xi_{0:k} \\ &\quad = \int \underbrace{\frac{p(T_{0:k}|\xi^i_{0:k})p(\xi^i_{0:k})}{p(T_{0:k})\pi(\xi^i_{0:k}|T_{0:k})}}_{w^{*i}_k}\delta(\xi_{0:k} - a^i_{0:k})\pi(\xi_{0:k}|T_{0:k})d\xi_{0:k} \end{aligned} \qquad (13)$$

After introducing importance function $\pi(a_{0:k}|T_{0:k})$, the estimate of posterior probability density can be written as

$$\begin{cases} \hat{p}^*(a_{0:k}|T_{0:k}) = \dfrac{1}{N}\displaystyle\sum_{1}^{N} w^{*i}_k\delta(a_{0:k} - a^i_{0:k}) \\ w^{*i}_k = \dfrac{p(T_{0:k}|a^i_{0:k})p(a^i_{0:k})}{p(T_{0:k})\pi(a^i_{0:k}|T_{0:k})} \end{cases} \qquad (14)$$

However,from the equation 13 and 14, the weight $w^i{}_k$ can be written as

$$w^i{}_k = w^{*i}_k p(T_{0:k}) = \frac{p(T_{0:k}|a^i_{0:k})p(a^i_{0:k})}{\pi(a^i_{0:k}|T_{0:k})} \qquad (15)$$

Therefore, the following equation can be obtained from Equation 14, 15.

$$\hat{p}^*(a_{0:k}|T_{0:k}) = \frac{1}{N}\sum_{1}^{N}\frac{w^i_k}{p(T_{0:k})}\delta(a_{0:k} - a^i_{0:k}) \qquad (16)$$

$$\begin{aligned} p(T_{0:k}) &= \int p(a_{0:k})p(T_{0:k}|a_{0:k})da_{0:k} \\ &= \int \frac{p(T_{0:k}|a_{0:k})}{\pi(a_{0:k}|T_{0:k})}p(a_{0:k})\pi(a_{0:k}|T_{0:k})da_{0:k} \end{aligned} \qquad (17)$$

Then the estimated value of the required time T can be written as Equation 18

$$\hat{p}(T_{0:k}) \approx \frac{1}{N}\sum_{1}^{N} w^i_k\delta(a_{0:k} - a^i_{0:k}) \qquad (18)$$

The following equations can be obtained from Equation 16 and Equation 18.

$$\begin{aligned}\hat{p}^*(a_{0:k}|T_{0:k}) &\approx \frac{1}{N}\sum_{1}^{N}\frac{w_k^i}{\hat{p}(T_{0:k})}\delta(a_{0:k}-a_{0:k}^i)\\ &= \frac{1}{N}\sum_{1}^{N}\frac{w_k^i}{\frac{1}{N}\sum_{1}^{N}w_k^i\delta(a_{0:k}-a_{0:k}^i)}\delta(a_{0:k}-a_{0:k}^i)\\ &= \sum_{1}^{N}\underbrace{\frac{w_k^i}{\sum_{1}^{N}w_k^i}}_{\tilde{w}_k^i}\delta(a_{0:k}-a_{0:k}^i) \end{aligned} \tag{19}$$

Then obtain the k-th time step distribution $p(a_{0:k}|T_{0:k})$ from the previous distribution according to the following recursive equations.

$$\begin{aligned}&p(a_{0:k}|T_{0:k})\\ &= \frac{p(a_k|a_{0:k-1},T_{0:k-1})\,p(a_{0:k-1}|T_{0:k-1})\,p(T_k|a_{0:k},T_{0:k-1})}{p(T_k|T_{0:k-1})}\\ &= p(a_{0:k-1}|T_{0:k-1})\frac{p(T_k|a_{0:k})\,p(a_k|a_{0:k-1})}{p(T_k|T_{0:k-1})}\end{aligned} \tag{20}$$

If the importance function π is selected as

$$\pi(a_{0:k}|T_{0:k})=\pi(a_k|a_{0:k-1},T_{0:k})\pi(a_{0:k-1}|T_{0:k-1}) \tag{21}$$

The weights $\tilde{w}_k$ can be obtained according to Equation 15 and Equation 19.

$$\begin{aligned}\tilde{w}_k^i &= w_k^{*i}p(T_{0:k})\\ &= \frac{p(a_{0:k}^i|T_{0:k})}{\pi(a_{0:k}^i|T_{0:k})}p(T_{0:k})\\ &= \frac{p(a_{0:k-1}^i|T_{0:k-1})\,p(T_k|a_k^i)\,p(a_k^i|a_{k-1}^i)}{\pi(a_k^i|a_{0:k-1}^i,T_{0:k})\pi(a_{0:k-1}^i|T_{0:k-1})p(T_k|T_{k-1})}\\ &= w_{k-1}^i\frac{p(T_k|a_k^i)\,p(a_k^i|a_{k-1}^i)}{\pi(a_k^i|a_{0:k-1}^i,T_{0:k})}\end{aligned} \tag{22}$$

The importance function $\pi(a_k|a_{0:k-1}^i,T_{0:k})=p(a_k|a_{k-1}^i)$ is usually chosen in practical engineering [32]–[34], therefore, the weight recursion Equation 23 can be obtained.

$$w_k^i = w_{k-1}^i p(T_k|a_k^i) \tag{23}$$

C. THE RESAMPLING

However, as the experiment progressed, the importance weights will gradually concentrate on a few random number samples, so the resampling is required, discarding random numbers with small weights, and copy those random numbers with strong weights, usually he threshold can be set here according to actual needs, (e.g., the effective random number is less than 75% of the number of particles). The resampling methods include random resampling, polynomial resampling, system resampling, residual resampling, reallocation resampling layered resampling, and various derivative re-sampling methods. Each resampling method also has its own advantages and disadvantages.

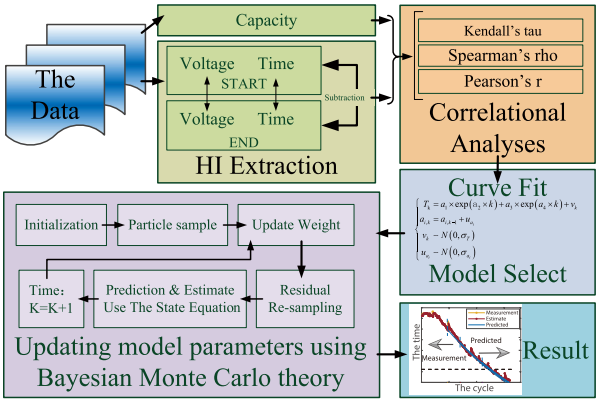

FIGURE 13. The flowchart of the proposed experiment scheme.

In this paper, residual resampling methods are used to resolve the degradation problem of random particles [35], [36]. The idea of residual resampling is to resample the integer part and fractional part separately. the number of runs will be less. There are 3 steps in residual resampling method:

step 1: Obtain $\{\overline{N}^i\}_{a\le i\le N}$ from $Mult(N-R;\overline{w}^1\ldots\overline{w}^N)$
Here, $R=\sum_{n=1}^{N}(Floor(Nw^i))$, $\overline{w}^i=\frac{Nw^i-Floor(Nw^i)}{N-R}$
Here, the $Floor$ is the integer arithmetic.
step 2: $N^i = Floor(Nw^i)+\overline{N}^i$
step 3: Redistribute the weight of each sample $\tilde{w}^i = 1/N$

D. THE SOH PROGNOSTICS

In this paper, the Bayesian Monte Carlo theory (BMC) is used to estimation of the time during which the lithium battery can be discharged in the future cycle, the N future state can be estimated using N sample random numbers a_k^i, so, the SOH of the lithium battery can be evaluated using this principle [3]. According to Equation 7 and Equation 23, the N-step forward prediction of the time required variable in this experiment can be calculated according to the following equation, and the SOH of the lithium battery can be judged according to the threshold Pre-set by the user.

$$\begin{aligned}\overline{T}_{k+p} &= \sum_{1}^{N}T_{k+p}^i\\ &= \sum_{1}^{N}w_k^i\begin{bmatrix}a_{1,k}^i\times\exp\left(a_{2,k}^i\times(k+p)\right)\\ +a_{3,k}^i\times\exp\left(a_{4,k}^i\times(k+p)\right)\end{bmatrix}\end{aligned} \tag{24}$$

Based on the dischargeable time series health indicator, the SOH of the batteries are predicted and estimated by using the Bayesian Monte Carlo theory, the flowchart of the experiment scheme proposed in this paper is shown in Fig.13.

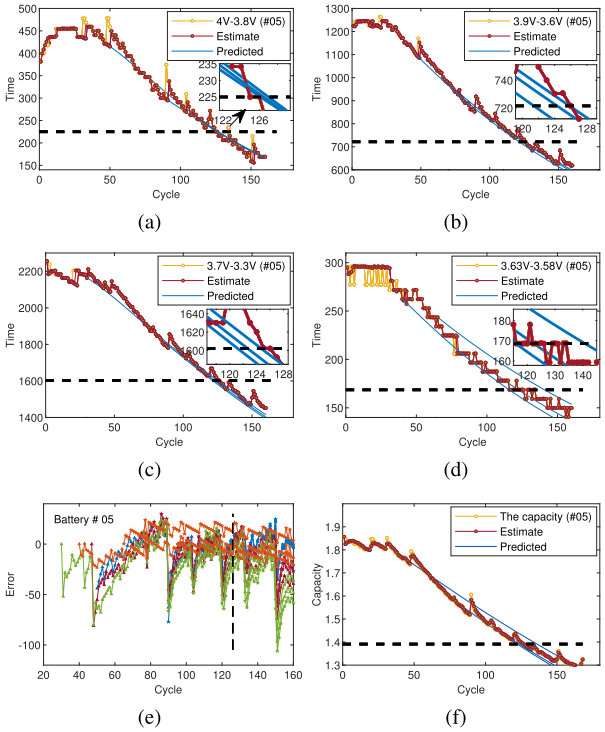

FIGURE 14. Prediction results: (a) 4V-3.8V (b) 3.9V-3.6V (c) 3.7V-3.3V (d) 3.63V-3.58V (e) Errors in figures14a ∼ 14d (f) Prediction based on capacity.

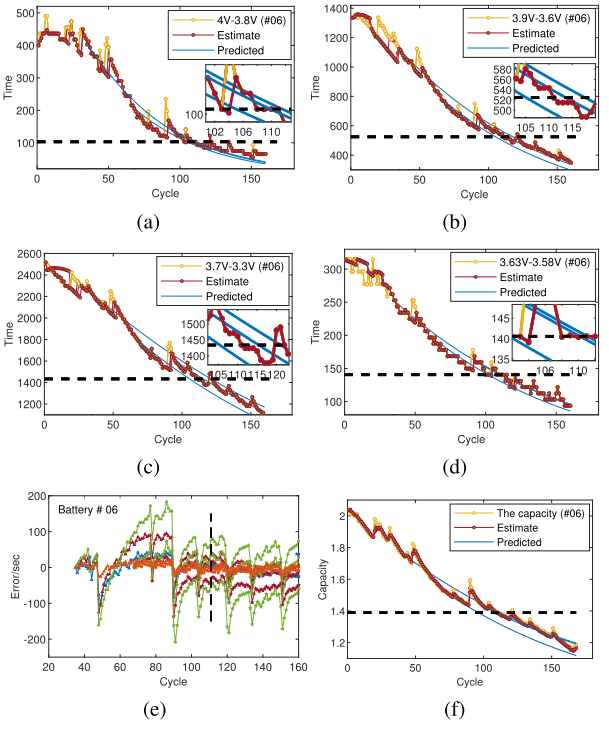

FIGURE 15. Prediction results: (a) 4V-3.8V (b) 3.9V-3.6V (c) 3.7V-3.3V (d) 3.63V-3.58V (e) Errors in figures 15a ∼ 15d (f) Prediction based on capacity.

V. EXPERIMENT RESULTS

A. EXPERIMENTS BASED ON DISCHARGE TIME HEALTH INDICATORS

Based on the dischargeable time-series health indicator, the SOH of the four batteries (#05, #06, #07 and #18) are estimated by using the Bayesian Monte Carlo theory. In order to compare the effect of predicting by using this scheme, the capacity was also selected as a health indicator and experiments were performed using the same algorithm.

Three different cycles were randomly selected as a starting point for prediction experiments, a total of 15 experiments per each battery, the 60 experimental results are shown in Fig.14 ∼ 17, and the unit of time is Seconds, the unit of capacity is Ampere-hour, besides, in the legend, predicted indicates that a different starting point is selected for prediction, estimate represents using the previous data to predict the next data. The detailed analysis is in Section VI (Discussion).

In Fig.14 and 15, the Figures14a ∼ 14d and Fig.15a ∼ 15d are experimental results based on the time required series for the battery #05 and #06, the prediction error is shown in Fig.14e and Fig.15e, the common BMC-based capacity degradation prediction result shows in Fig.14f and Fig.15f. In the experiments of these two batteries, four voltage drops of 4V-3.8V, 3.9V-3.6V, 3.7V-3.3V and 3.63V-3.58V are selected respectively, the dotted line represents the end of life (EOL).

The experimental results of battery #07 and battery #18 are shown in Fig.16 ∼ 17. To research the prediction effect

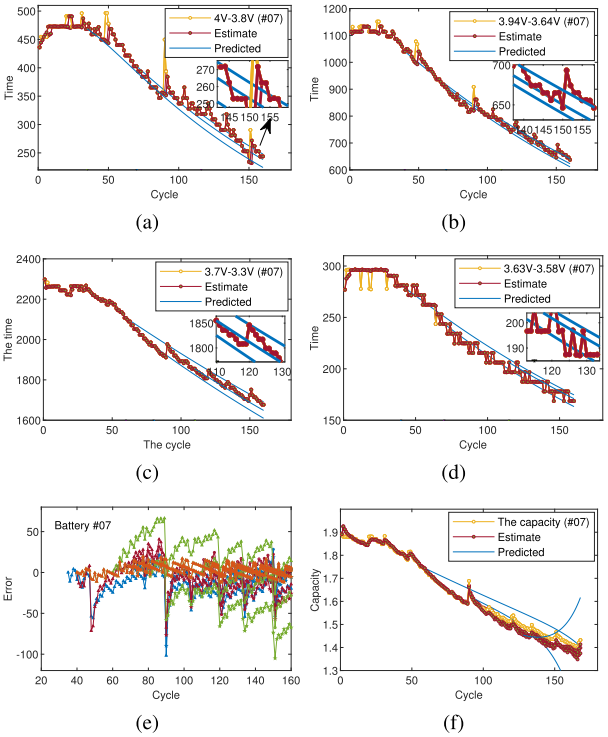

FIGURE 16. Prediction results: (a) 4V-3.8V (b) 3.94V-3.64V (c) 3.7V-3.3V (d) 3.63V-3.58V (e) Errors in figures 16a ∼ 16d (f) Prediction based on capacity.

of non-integer voltage ranges, the experimental scheme of these two batteries has been slightly modified. we select the voltage was dropped from 3.94V to 3.64V(battery #07) and

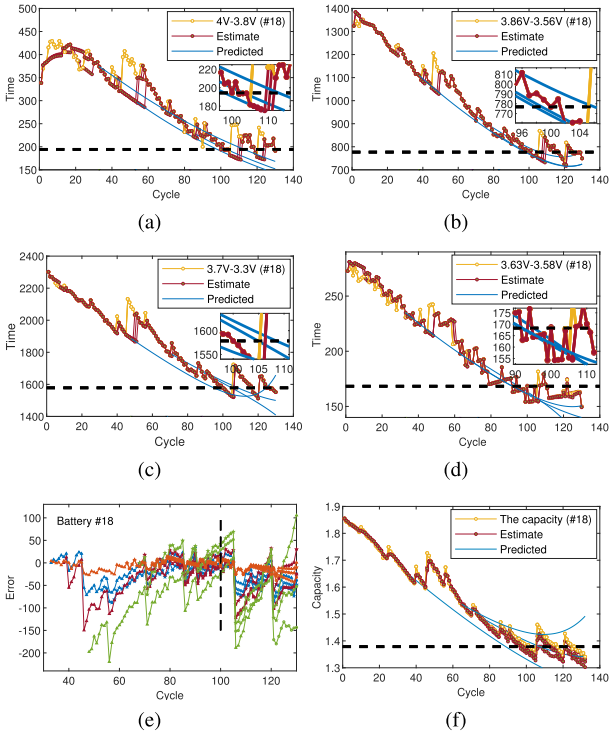

FIGURE 17. Prediction results: (a) 4V-3.8V (b) 3.86V-3.56V (c) 3.7V-3.3V (d) 3.63V-3.58V (e) Errors in figures 17a∼ 17d (f) Prediction based on capacity.

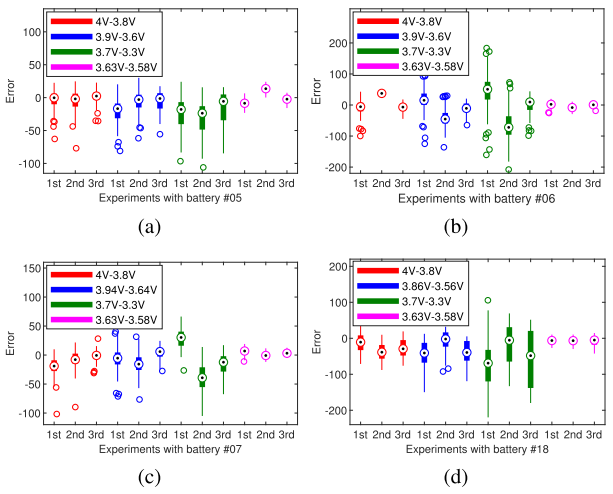

FIGURE 18. Boxplots of the error (error = x* − x): (a) #05 (b) #06 (c) #07 (d) #18.

3.86V to 3.56V(#18), the experiments results correspond to Fig.16b ∼ 17b. Compared with Fig.14b ∼ 15b, although the voltage drop is still 0.3V, the voltage ranges are changed, in other cases, the experimental scheme was the same as that of battery #05 and #06. The boxplot of error is shown in Fig.18.

B. EXPERIMENTS BASED ON CHARGE TIME HEALTH INDICATORS

Similar to SectionV-A, using the charge time difference health indicator to conduct experiments. The three voltage

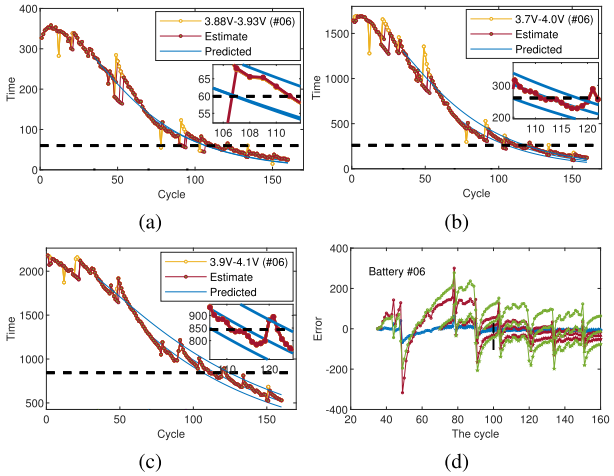

FIGURE 19. Experiment results of battery #06: (a) 3.88V-3.93V (b) 3.7V-4.0V (c) 3.9V-4.1V (d) Error.

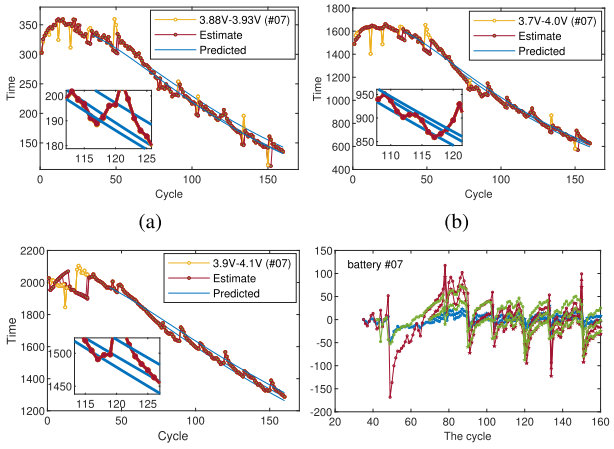

FIGURE 20. Experiment results of battery #07: (a) 3.88V-3.93V (b) 3.7V-4.0V (c) 3.9V-4.1V (d) Error.

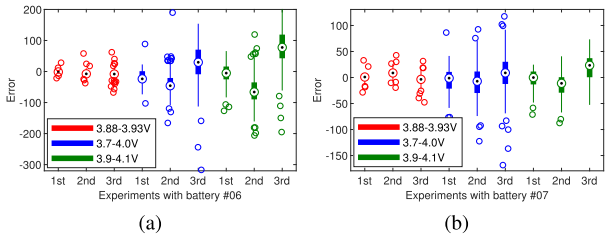

FIGURE 21. Prediction results: (a) boxplot battery #06 (b) boxplot battery #07.

range corresponding to the health indicator in the experiment is 3.8-3.93V, 3.7-4.0V, 3.9-4.1V, respectively. Choose battery 06 and 07, randomly select 3 different cycles as the starting point, a total of 18 experimental results are shown in Fig.19 and 20, the boxplot of error is shown in Fig.21.

C. EXPERIMENTS BASED ON HYBRID HEALTH INDICATORS

Similar to the above, using the hybrid health indicators to experimental. The corresponding voltage ranges

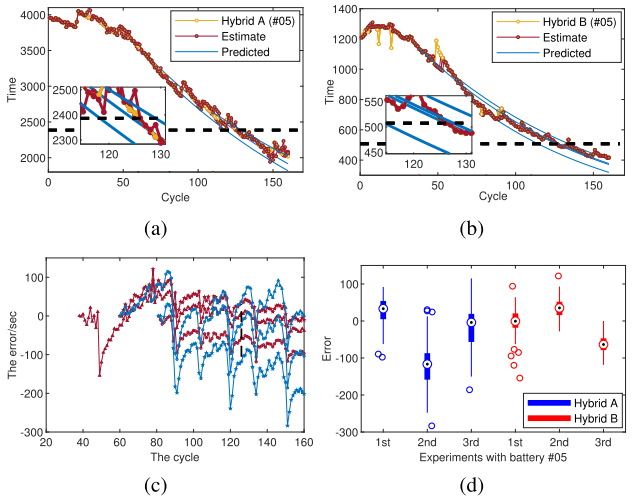

FIGURE 22. Prediction results #05: (a) Hybrid health indicators A (b) Hybrid health indicators B (c) Errors (d) Boxplot.

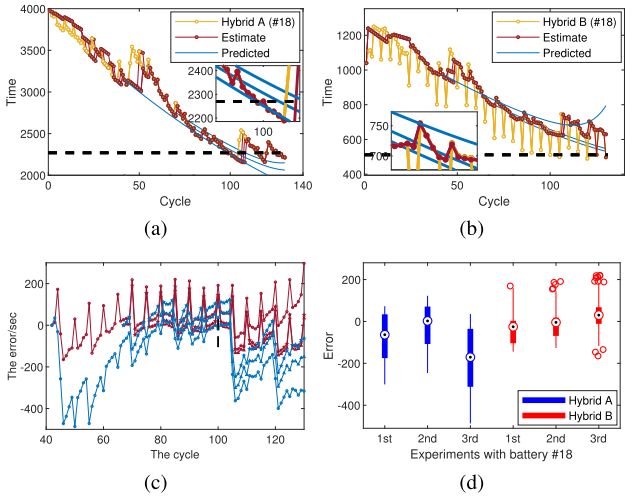

FIGURE 23. Prediction results #18: (a) Hybrid health indicators A (b) Hybrid health indicators B (c) Errors (d) Boxplot.

are **A**: 3.9V-4.1V/3.7-3.4V and **B**: 3.9V-3.7/3.7V-3.9V, respectively. Select battery #05 and #18, randomly use 3 cycles as the starting point of the experiment, a total of 12 experiments results are shown in Fig.22 and 23. The experimental errors and box plots are also given, same as above.

VI. DISCUSSION

A. DISCUSSION ABOUT DISCHARGE TIME HEALTH INDICATOR

In Section V, the experimental results of state prediction of discharge time for battery (#05, #06, #07 and #18) in the future based on time required for a voltage drop of 0.2 volts as a health indicator are shown in Fig.14 ∼ 17, respectively.

Since the capacity degradation of battery #07 in battery raw dataset does not reach the threshold of 1.38V, therefore, the threshold dotted line is not shown in the experimental results of battery #07. The dotted lines are experimental

TABLE 11. The values of the boxplots & means(Fig 18a).

Voltage Range		25∼75%	Mean
4V∼3.8V	1st	-10.0952∼5.9909	-0.24744s
	2nd	-13.6467∼6.0619	-1.9397s
	3rd	-3.583∼8.1436	2.3589s
3.9V∼3.6V	1st	-31.3643∼-8.9284	-16.751s
	2nd	-14.9461∼4.4573	-2.9839s
	3rd	-16.5876∼6.7891	-1.3387s
3.7V∼3.3V	1st	-40.2995∼-6.8211	-17.9177s
	2nd	-48.5748∼12.9916	-23.7273s
	3rd	-34.4035∼4.8639	-5.6632s
3.63V∼3.58V	1st	-12.7453∼-4.2076	-8.5736s
	2nd	9.1453∼16.9878	-13.5749
	3rd	-6.8003∼0.72181	-2.3461s

results near the end of life, and this accuracy can meet the practical application. To further analyze the characteristics of the experiment error. In Fig. 14e, 15e, 16e and 17e, a total of 48 curves (each curve represents the error from the beginning to the end in each experiment) are drawn as 48 boxplots in Fig.18a, 18b, 18c and 18d. Because the time difference corresponding to different voltage differences in the figure is different, taking the maximum 0.4V voltage drop and the minimum 0.05V voltage drop as examples, the time corresponding to 0.4V voltage drop is from about 2400 seconds to about 1500 seconds, but the time corresponding to 0.05V voltage drop is from about 300s to about 150s.

To observe the error after multiple experiments, errors of 12 predictions are drawn together (Figures 14e, 15e, 16e and 17e), since it is difficult to label legend here, the explained as follows, the ordinate is the error (unit is seconds), four colors represent four different voltage drops selected, three symbols on the curve represent three predictions, the abscissa of the curve represents the number of cycles. It can be clearly seen from Figures 14e, 15e, 16e and 17e and Fig.18 that, since the length of time required for different discharge voltage drops is different, the error is different.

Take Battery #05 as an example (Fig.14e and 18a), it is obvious from 12 boxplots that the range between 25th percentiles and 75th percentiles is also small, the values in the 12 boxplots are shown in table 11, a similar conclusion can be drawn from the analysis of battery #06 (Fig.15e, Fig.18b), battery07 (Fig.16e, Fig.18c), and battery18 (Fig.17e, Fig.18d).

Finally, from the experimental error box diagram, it can be found that the error outliers of the experimental results are related to the correlation of the health indicator. The lower the correlation coefficient, the more the error outliers.

B. DISCUSSION ABOUT CHARGE TIME HEALTH INDICATOR

The experimental results based on the charging time health indicator are shown in Fig.19, 20, and 21. Three Figures are the experimental results of #06, #07 and the box plots of errors, respectively. From the experiment, it can be seen that not only the discharge time can characterize the health of

the battery, but also the charging time can also characterize the health of the battery, but the interval of the best time health indicator is different. From Fig. 4, Fig. 5 and sectionIII-D, it can be known that there is an interval similar to the discharge plateau period during the charging process, which is approximately 3.9V to no more than 4.2V. After 4.2V, the voltage stabilizes at 4.2V and continues to constant voltage charging. Other analysis is similar to sectionVI-A.

C. DISCUSSION ABOUT HYBRID HEALTH INDICATOR

It can be seen from the experiment that the Hybrid health indicator that integrates the discharge process and the charging process also well characterizes the health status of the battery. In addition, it can be seen from his Fig.22 and 23 that not only the error is related to the interval of the time health indicator, but also closely related to its correlation. Because the Hybrid health indicator B combines the best charging time state and the non-optimal discharging time, the effect of Hybrid health indicator B is slightly worse than A, especially in the Fig.23b, that is, the outliers of indicator B are more than A in the boxplot (red circle). Other analysis is similar to sectionVI-A

VII. CONCLUSION

Generally, the health monitoring and RUL prediction of lithium batteries are mainly estimated by calculating the attenuation of the accumulated discharge power amount per cycle in the past, which is not suitable for practical applications. In this paper, from the perspective of time, this paper analyzes the relationship between three types of time health indicators and capacity decline.To evaluate the prediction effect based on time health indicator, the Bayesian Monte Carlo theory is used to predict the future discharge time of lithium batteries.

The research results show that the dischargeable time/charging time of lithium batteries in each cycle is highly correlated with the health status of lithium batteries. According to the actual demand, the time series of the voltage discharge platform period can be used as a health indicator to characterize the degradation of lithium batteries, and the closer to the center of the platform period, the better the prediction effect. The charging process is similar to the discharging process, and the Hybrid time health indicator combined with the charging and discharging process can also achieve the same effect. Also, the prediction of BMC based on time health indicator can well estimate and predict the SOH of lithium batteries. This scheme can directly evaluate the State of lithium battery by the discharge time, and directly obtain the predicted dischargeable time of the battery in the future, and can also estimate the capacity.

From a quantitative perspective, the prediction method based on capacity as a health indicator mainly rely on the voltage drop from 4.2V to 2.7V, the max difference is only 1.5V, but from time perspective, the same sampling frequency, the discharge time in NASA battery dataset is from a minimum of about 9 seconds to maximum of nearly 4000 seconds, the time difference magnitude is thousands of times the magnitude of voltage difference, the reflection effect of deterioration is more significant. The other two types of health indicators have similar conclusions.

Therefore, the method proposed in this paper has certain application value in situations where high-precision test equipment cannot be used to evaluate the SOH of battery, such as mobile devices, drones, and electric vehicle testing.In our future research, considering the high-precision health indicator of lithium batteries under random conditions, more efficient prediction methods and the more accurate model of lithium battery degradation will be further studied.

NOMENCLATURE

SOH	State Of Health
RUL	Remaining Useful Life
SSE	Sum of squares for error
SST	Sum of squares for total
RMSE	Root mean squared error
R^2_{adj}	R-squared adjusted
Kendall's tau	Kendall's tau correlation coefficient
Pearson's r	Pearson's linear correlation coefficient
Spearman's rho	Spearman's rank correlation coefficient

REFERENCES

[1] B. Saha, K. Goebel, S. Poll, and J. Christophersen, "Prognostics methods for battery health monitoring using a Bayesian framework," *IEEE Trans. Instrum. Meas.*, vol. 58, no. 2, pp. 291–296, Feb. 2009, doi: 10.1109/TIM.2008.2005965.

[2] B. Saha, K. Goebel, and J. Christophersen, "Comparison of prognostic algorithms for estimating remaining useful life of batteries," *Trans. Inst. Meas. Control*, vol. 31, nos. 3–4, pp. 293–308, Jun. 2009, doi: 10.1177/0142331208092030.

[3] W. He, N. Williard, M. Osterman, and M. Pecht, "Prognostics of lithium-ion batteries based on Dempster–Shafer theory and the Bayesian Monte Carlo method," *J. Power Sour.*, vol. 196, no. 23, pp. 10314–10321, 2011, doi: 10.1016/j.jpowsour.2011.08.040.

[4] D. Wang, Q. Miao, and M. Pecht, "Prognostics of lithium-ion batteries based on relevance vectors and a conditional three-parameter capacity degradation model," *J. Power Sour.*, vol. 239, pp. 253–264, Oct. 2013, doi: 10.1016/j.jpowsour.2013.03.129.

[5] Y. Xing, E. W. M. Ma, K.-L. Tsui, and M. Pecht, "An ensemble model for predicting the remaining useful performance of lithium-ion batteries," *Microelectron. Rel.*, vol. 53, pp. 811–820, Jun. 2013, doi: 10.1016/j.microrel.2012.12.003.

[6] D. Liu, H. Wang, Y. Peng, W. Xie, and H. Liao, "Satellite lithium-ion battery remaining cycle life prediction with novel indirect health indicator extraction," *Energies*, vol. 6, no. 8, pp. 3654–3668, Jul. 2013, doi: 10.3390/en6083654.

[7] C. Hu, G. Jain, P. Tamirisa, and T. Gorka, "Method for estimating capacity and predicting remaining useful life of lithium-ion battery," *Appl. Energy*, vol. 126, pp. 182–189, Aug. 2014, doi: 10.1016/j.apenergy.2014.03.086.

[8] D. Liu, J. Zhou, H. Liao, Y. Peng, and X. Peng, "A health indicator extraction and optimization framework for lithium-ion battery degradation modeling and prognostics," *IEEE Trans. Syst., Man, Cybern. Syst.*, vol. 45, no. 6, pp. 915–928, Jun. 2015, doi: 10.1109/TSMC.2015.2389757.

[9] D. Liu, W. Xie, H. Liao, and Y. Peng, "An integrated probabilistic approach to lithium-ion battery remaining useful life estimation," *IEEE Trans. Instrum. Meas.*, vol. 64, no. 3, pp. 660–670, Mar. 2015, doi: 10.1109/TIM.2014.2348613.

[10] Y. Zhou, M. Huang, Y. Chen, and Y. Tao, "A novel health indicator for online lithium-ion batteries remaining useful life prediction," *J. Power Sour.*, vol. 321, pp. 1–10, Jul. 2016, doi: 10.1016/j.jpowsour.2016.04.119.

[11] S.-C. Huang, K.-H. Tseng, J.-W. Liang, C.-L. Chang, and M. Pecht, "An online SOC and SOH estimation model for lithium-ion batteries," *Energies*, vol. 10, no. 4, p. 512, Apr. 2017, doi: 10.3390/en10040512.

[12] X. Su, S. Wang, M. Pecht, L. Zhao, and Z. Ye, "Interacting multiple model particle filter for prognostics of lithium-ion batteries," *Microelectron. Rel.*, vol. 70, pp. 59–69, Mar. 2017, doi: 10.1016/j.microrel.2017.02.003.

[13] L. Ren, L. Zhao, S. Hong, S. Zhao, H. Wang, and L. Zhang, "Remaining useful life prediction for lithium-ion battery: A deep learning approach," *IEEE Access*, vol. 6, pp. 50587–50598, 2018, doi: 10.1109/ACCESS.2018.2858856.

[14] Y. Sun, X. Hao, M. Pecht, and Y. Zhou, "Remaining useful life prediction for lithium-ion batteries based on an integrated health indicator," *Microelectron. Rel.*, vols. 88–90, pp. 1189–1194, Sep. 2018, doi: 10.1016/j.microrel.2018.07.047.

[15] X. Han, L. Lu, Y. Zheng, X. Feng, Z. Li, J. Li, and M. Ouyang, "A review on the key issues of the lithium ion battery degradation among the whole life cycle," *ETransportation*, vol. 1, Aug. 2019, Art. no. 100005, doi: 10.1016/j.etran.2019.100005.

[16] J. Wei, G. Dong, and Z. Chen, "Remaining useful life prediction and state of health diagnosis for lithium-ion batteries using particle filter and support vector regression," *IEEE Trans. Ind. Electron.*, vol. 65, no. 7, pp. 5634–5643, Jul. 2018, doi: 10.1109/TIE.2017.2782224.

[17] Y. Sun, S. Saxena, and M. Pecht, "Derating guidelines for lithium-ion batteries," *Energies*, vol. 11, no. 12, p. 3295, Nov. 2018, doi: 10.3390/en11123295.

[18] S. Saxena, Y. Xing, D. Kwon, and M. Pecht, "Accelerated degradation model for C-rate loading of lithium-ion batteries," *Int. J. Electr. Power Energy Syst.*, vol. 107, pp. 438–445, May 2019, doi: 10.1016/j.ijepes.2018.12.016.

[19] J. Lee, D. Kwon, and M. G. Pecht, "Reduction of li-ion battery qualification time based on prognostics and health management," *IEEE Trans. Ind. Electron.*, vol. 66, no. 9, pp. 7310–7315, Sep. 2019, doi: 10.1109/TIE.2018.2880701.

[20] Y. Zhang, R. Xiong, H. He, and M. Pecht, "Validation and verification of a hybrid method for remaining useful life prediction of lithium-ion batteries," *J. Cleaner Prod.*, vol. 212, pp. 240–249, Mar. 2019, doi: 10.1016/j.jclepro.2018.12.041.

[21] Y. Zhang, R. Xiong, H. He, and M. G. Pecht, "Lithium-ion battery remaining useful life prediction with Box–Cox transformation and Monte Carlo simulation," *IEEE Trans. Ind. Electron.*, vol. 66, no. 2, pp. 1585–1597, Feb. 2019, doi: 10.1109/TIE.2018.2808918.

[22] F. Cadini, C. Sbarufatti, F. Cancelliere, and M. Giglio, "State-of-life prognosis and diagnosis of lithium-ion batteries by data-driven particle filters," *Appl. Energy*, vol. 235, pp. 661–672, Feb. 2019, doi: 10.1016/j.apenergy.2018.10.095.

[23] J. Zhu, Z. Sun, X. Wei, H. Dai, and W. Gu, "Experimental investigations of an AC pulse heating method for vehicular high power lithium-ion batteries at subzero temperatures," *J. Power Sour.*, vol. 367, pp. 145–157, Nov. 2017, doi: 10.1016/j.jpowsour.2017.09.063.

[24] B. Saha and K. Goebel, "Battery data set," NASA Ames Prognostics Data Repository, NASA Ames Res. Center, Moffett Field, CA, USA, Tech. Rep., [Online]. Available: https://ti.arc.nasa.gov/tech/dash/groups/pcoe/prognostic-data-repository/

[25] J. D. Gibbons and S. Chakraborti, *Nonparametric Statistical Inference*, 5th ed. Boca Raton, FL, USA: CRC Press, 2011, pp. 389–416.

[26] M.-T. Puth, M. Neuhäuser, and G. D. Ruxton, "Effective use of Pearson's product–moment correlation coefficient," *Animal Behav.*, vol. 93, pp. 183–189, Jul. 2014, doi: 10.1016/j.anbehav.2014.05.003.

[27] A. Doucet, S. Godsill, and C. Andrieu, "On sequential Monte Carlo sampling methods for Bayesian filtering," *Statist. Comput.*, vol. 10, no. 3, pp. 197–208, 2000, doi: 10.1023/A:1008935410038.

[28] M. S. Arulampalam, S. Maskell, N. Gordon, and T. Clapp, "A tutorial on particle filters for online nonlinear/non-Gaussian Bayesian tracking," *IEEE Trans. Signal Process.*, vol. 50, no. 2, pp. 174–188, 2002, doi: 10.1109/78.978374.

[29] G. Dong, Z. Chen, J. Wei, and Q. Ling, "Battery health prognosis using Brownian motion modeling and particle filtering," *IEEE Trans. Ind. Electron.*, vol. 65, no. 11, pp. 8646–8655, Nov. 2018, doi: 10.1109/TIE.2018.2813964.

[30] L. Zhang, Z. Mu, and C. Sun, "Remaining useful life prediction for lithium-ion batteries based on exponential model and particle filter," *IEEE Access*, vol. 6, pp. 17729–17740, 2018, doi: 10.1109/access.2018.2816684.

[31] D. Liu, X. Yin, Y. Song, W. Liu, and Y. Peng, "An on-line state of health estimation of lithium-ion battery using unscented particle filter," *IEEE Access*, vol. 6, pp. 40990–41001, 2018, doi: 10.1109/ACCESS.2018.2854224.

[32] F. Cadini, E. Zio, and D. Avram, "Monte Carlo-based filtering for fatigue crack growth estimation," *Probabilistic Eng. Mech.*, vol. 24, no. 3, pp. 367–373, Jul. 2009, doi: 10.1016/j.probengmech.2008.10.002.

[33] H. Tanizaki, "Nonlinear and nonnormal filters using Monte Carlo methods," *Comput. Statist. Data Anal.*, vol. 25, no. 4, pp. 417–439, 1997, doi: 10.1016/S0167-9473(97)00016-9.

[34] H. Tanizaki and R. S. Mariano, "Nonlinear and non-Gaussian state-space modeling with Monte Carlo simulations," *J. Econ.*, vol. 83, nos. 1–2, pp. 263–290, 1998, doi: 10.1016/S0304-4076(97)80226-6.

[35] T. Li, M. Bolic, and P. M. Djuric, "Resampling methods for particle filtering: Classification, implementation, and strategies," *IEEE Signal Process. Mag.*, vol. 32, no. 3, pp. 70–86, May 2015, doi: 10.1109/MSP.2014.2330626.

[36] T.-C. Li, G. Villarrubia, S.-D. Sun, J. M. Corchado, and J. Bajo, "Resampling methods for particle filtering: Identical distribution, a new method, and comparable study," *Frontiers Inf. Technol. Electron. Eng.*, vol. 16, no. 11, pp. 969–984, Nov. 2015, doi: 10.1631/FITEE.1500199.

ZHONGHUA YUN received the M.S. degree from Southwest Jiaotong University, Chengdu, China, in 2012. He is currently pursuing the Ph.D. degree with Southeast University, Nanjing, China. Since 2014, he has been working with Tibet University, Lhasa, where he has also been serving as a Lecturer with the School of Engineering, since 2015. His current research interests include vehicle safety monitoring, signal processing, and control technology.

WENHU QIN received the Ph.D. degree from Southeast University, Nanjing, China, in 2005. From 2009 to 2010, he was a Visiting Scholar with the University of Pennsylvania. He was a Senior Visiting Scholar with the University of California at Berkeley, Berkeley, in 2014. He is currently a Professor with the School of Instrument Science and Engineering, Southeast University, where he has been on the faculty, since 1997. He is also the Director of the Jiangsu Agricultural IoT Perception and Control Engineering Laboratory and the Deputy Director of the Suzhou Automotive Electronics and Intelligent Transportation Key Laboratory. Since 2018, he has been serving as the Vice President of the Wuxi Branch, Southeast University. He has authored or coauthored about 60 articles and a book. His research interests include vehicle safety, vehicle electronics control technology, and road traffic accident reconstruction. He has also served as a reviewer for many well-known journals, such as the IEEE TRANSACTIONS ON INTELLIGENT TRANSPORTATION SYSTEMS.